43rd AIAA Aerospace Sciences Meeting and Exhibit, 10-13 Jan 2005, Reno, NV

An Unsteady/Flamelet Progress Variable Method for LES of Nonpremixed Turbulent Combustion

Heinz Pitsch* and Matthias Ihme†

Stanford University, Stanford, CA 94305, USA

An unsteady flamelet/progress variable model has been developed and formulated as an extension of the steady flamelet/progress variable model. For this model, a large number of unsteady laminar flamelet simulations is performed for various conditions, and solutions are recorded as function of time. From this, a flamelet library is generated, which provides the filtered quantities of all scalar values as function of the filtered mixture fraction, the mixture fraction sub-filter variance, the filtered reaction progress variable, and the filtered scalar dissipation rate. The model has been implemented in an LES code. Simulations have been performed for a confined swirl burner using the unsteady flamelet/progress variable model. The results are compared with experimental data for velocities and velocity fluctuations, temperature, CO_2, and CO mole fractions. The results agree reasonably well with the experiments for all quantities. In particular, CO is predicted with good accuracy.

I. Introduction

One of the main challenges in aircraft engine design is the joint optimization of pollutant emissions, efficiency, and stability of the combustion process. The main reason why stationary gas turbines for power generation are operated at lean conditions is that regions of high fuel/air ratio at about stoichiometric conditions burn at high temperatures, which strongly promotes the production of oxides of nitrogen (NO_x) owing to its exponential temperature dependence. Different concepts for the reduction of mainly NO_x, but also soot, have been proposed, which are usually based on highly diluted lean combustion to decrease the temperature. However, for aircraft engines, the lean combustion concept cannot be employed, since stability has to be ensured for a wide range of operating conditions. Another viable approach is the rich-burn-quick-quench-lean-burn method, where an initial rich burning phase ensures the desired stability at moderately low temperatures. In this rich region the fuel is essentially converted to CO. The subsequent fast mixing with air to lean conditions prevents burning at stoichiometric condition at high temperatures and supposedly ensures burnout of CO and soot. It is obvious that this mixing process is of particular importance for the emissions of pollutants and for engine performance.

Currently, the desired stability and robustness can only be assured by combustion with at least locally high fuel/air ratio. The pacing item for low emissions, good performance, and low pattern factor is hence the understanding and control of the rich combustion chemistry and the complex mixing process. Because of the strongly swirling flow, the occurrence of multiple recirculation regions, and mixing with secondary air in the form of jets in cross-flow, the flow field dynamics and the mixing cannot be described with sufficient accuracy by Reynolds averaged Navier Stokes (RANS) methods. Large eddy simulations using sophisticated combustion models, however, have been shown to predict stable intermediate species, such as CO, in this type of flow with high accuracy.[1] Present and future engine design strategies will still largely rely on RANS simulations, but in order to optimize and control complex combustion processes, it will be essential to have improved predictive accuracy. LES will also play an important role in the understanding of the relevant interaction of fluid dynamics and chemistry because of the high degree of detail obtained from these simulations.

*Assistant Professor, Department of Mechanical Engineering, Stanford University, AIAA member

†Research Assistant, Department of Mechanical Engineering, Stanford University

The purpose of this paper is to develop and test a combustion model that is accurate enough to predict the heat release, dynamic combustion behavior, and also stable intermediates such as carbon monoxide, but which is at the same time straightforward to implement and does not significantly increase computational times. The Flamelet/Progress Variable (FPV) approach, developed as a combustion model for LES by Pierce and Moin,[2,3] has been shown to predict the heat release in aircraft engine type combustors rather adequately. However, earlier validation studies have shown that CO has not been predicted with sufficient accuracy. The FPV model is constructed as follows. All filtered scalar quantities are evaluated from the convolution of a steady flamelet library with a presumed joint probability density function (pdf) of the mixture fraction Z and a flamelet parameter λ, which is determined from a reaction progress variable. Hence, the flamelet library also has to be parameterized by the mixture fraction and the flamelet parameter. A transport equation is solved for the filtered reaction progress variable. The filtered chemical source term appearing in this equation is also determined from the flamelet library. The great advantage of this formulation is that expressing the flamelet parameter by the reaction progress variable allows for the description of local extinction and reignition, and of partially premixed combustion, such as in lifted flames. However, in the present form, this model involves several assumptions. For the evaluation of the filtered chemical source term, in addition to the flamelet assumption, it is assumed that mixture fraction and flamelet parameter are uncorrelated, that the pdf of the flamelet parameter is given by a delta-function, and that the pdf of the mixture fraction is given by a beta-function.

The model proposed here is an extension of the Flamelet/Progress Variable (FPV) approach, but is re-formulated to consider the unsteadiness of the flame structure. This extension is motivated by our earlier DNS studies,[4] where we found that one of the main sources of uncertainty is the unsteadiness of the flame structure, which is not captured with the steady state flamelet libraries. We have also shown in the past that LES using unsteady flamelet models can be very accurate for CO predictions.[5] The main feature of the model extension is that the Unsteady Flamelet/Progress Variable (UFPV) approach presented here is based on an unsteady flamelet method. A flamelet library is constructed from the solutions of unsteady laminar flamelets. This introduces the scalar dissipation rate as an additional parameter for the flamelet library.

II. Model Development

A. Flamelet/Progress Variable Model

The flamelet model[6,7] considers a turbulent diffusion flame as an ensemble of laminar flamelets. This model introduces the mixture fraction Z as a conserved scalar. The species mass fractions and temperature are related to the mixture fraction by the solution of the flamelet equations. A parameter appearing in this model is the dissipation rate χ of the conserved scalar, defined as

$$\chi = 2D_Z(\nabla Z)^2 \,, \tag{1}$$

where D_Z is the molecular diffusivity of the mixture fraction. The steady flamelet equations are given by

$$-\rho\frac{\chi}{2}\frac{\partial^2\boldsymbol{\phi}}{\partial Z^2} = \boldsymbol{\omega} \,, \tag{2}$$

where the scalar dissipation rate appears as an external parameter. In Eq. 2, ρ is the density, $\boldsymbol{\phi}$ is the vector of species mass fractions and temperature, and $\boldsymbol{\omega}$ denotes their respective source terms. Assuming a unique functional dependence of the scalar dissipation rate on the mixture fraction, the state relation given by Eq. 2 can be written in the form

$$\boldsymbol{\phi} = \boldsymbol{\phi}(Z, \chi_{\rm st}) \,, \tag{3}$$

where $\chi_{\rm st}$ is the scalar dissipation rate at stoichiometric mixture fraction, $Z_{\rm st}$. The solution of the flamelet equations can be represented by the so-called S-shaped curve, which shows the stoichiometric temperature as function of the stoichiometric scalar dissipation rate. As an example, the S-shaped curve for the experiment considered below is shown in Fig. 1.

The upper and lower branches of this curve describe the stable burning and non-burning solutions, respectively. The middle solution branch is unstable. The turning point between the upper and middle branches corresponds to $\chi = \chi_{\rm q}$. Since multiple solutions exist for certain values of the dissipation rate, a unique parameterization of the flamelet solutions in terms of the scalar dissipation rate cannot represent the entire solution space. Typically, in applications of the flamelet model, only the burning branch of the

S-shaped curve is considered. Even if the lower branch of the non-burning solutions is also considered for $\chi > \chi_q$, it is obvious that there exists a discontinuity in the solution at $\chi = \chi_q$ and intermediate states of the reactive scalar between fully burning and fully extinguished cannot be described. This implies that any physical state between the fully burning and extinguished state in the steady state flamelet model will be projected onto the burning or the non-burning solution, depending on the value of the stoichiometric scalar dissipation rate. Hence, the flamelet model, parameterized with the scalar dissipation rate, corresponds to a projection of the state at constant scalar dissipation rate onto the S-shaped curve.

The flamelet/progress variable approach introduces a new flamelet parameter λ, which is based on a reactive scalar. The state of the flame is then parameterized by the flamelet parameter λ rather than the scalar dissipation rate, which uniquely identifies each single flame state along the S-shaped curve, including the unstable branch. Flamelets experiencing a transition from the burning to the extinguished flame state, or those which are likely to re-ignite, are then projected horizontally onto the S-shaped curve. The flamelet parameter λ is defined through a reactive scalar C, which has been introduced by Pierce & Moin[2,3] to be a linear combination of major reaction products. In the present work, we choose C to be the sum of the mass fractions of CO_2, H_2O, CO, and H_2. Then, the flamelet parameter λ at any state given by Z and C is defined to be the corresponding progress variable at stoichiometric mixture fraction determined using the flamelet library. An example for a specific stoichiometric scalar dissipation rate is shown in Fig. 2. Any local combination of mixture fraction and progress variable corresponding to that flamelet is described by the flamelet parameter λ indicated in that figure. This implies that the value of λ is a given value for a given flamelet and therefore independent of the mixture fraction. We can then express the solutions of Eq. 2 in terms of λ as

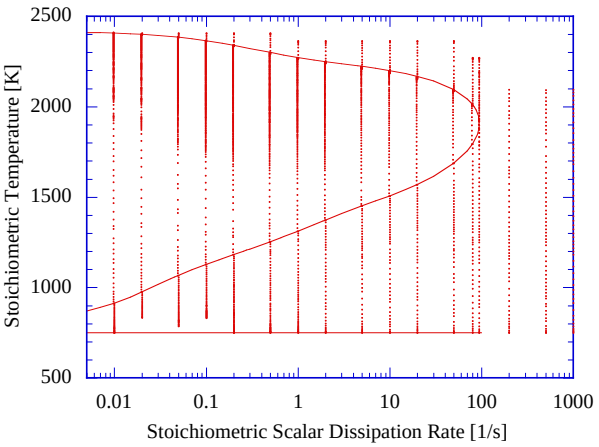

Figure 1. Stoichiometric temperature as function of stoichiometric scalar dissipation rate from the unsteady flamelet library. Solid line is S-shaped curve for steady state solutions of the flamelet equations for methane at atmospheric pressure and $T_{air} = 750$ K. Vertical dotted lines correspond to unsteady flamelet solutions for same conditions. Each point corresponds to a flamelet solution used in the construction of the unsteady flamelet library.

$$\boldsymbol{\phi} = \boldsymbol{\phi}(Z, \lambda) \ , \tag{4}$$

where $\boldsymbol{\phi}(Z, \lambda)$ is given by the steady flamelet solutions. Note that this is different from Eq. 3, as it includes all solutions of the steady state flamelet equations. For any given combination of Z and C, λ can be determined by inverting Eq. 4, which assumes that a unique inversion exists. It is interesting to note that if a turbulent reactive flow can be described by Eq. 4, meaning that all flame states correspond to solutions of the steady flamelet equations, then Z and λ are independent due to the choice of the definition of λ. This is an important property, since it simplifies the modeling of the joint PDF of Z and λ.

Without further assumptions, the mean values of the scalars $\boldsymbol{\phi}$ can be determined from

$$\widetilde{\boldsymbol{\phi}}(t, \boldsymbol{x}) = \int_{\lambda^-}^{\lambda^+} \int_0^1 \boldsymbol{\phi}(Z, \lambda) \widetilde{P}(Z, \lambda; t, \boldsymbol{x}) dZ d\lambda \ , \tag{5}$$

where $\widetilde{P}(Z, \lambda; t, \boldsymbol{x})$ is the Favre joint PDF of Z and λ. The integration limits λ^+ and λ^- correspond to the solution of Eq. 2 for $\chi_{st} \to 0$ and $\chi_{st} \to \infty$, respectively. In turbulent combustion, the PDF of any scalar is a function of space and time. In the following, for simplicity of notation, we will not write the implicit dependence on $\boldsymbol{x}$ and t. Using Bayes' theorem, the joint PDF can be written in terms of a conditional PDF, $\widetilde{P}(\lambda|Z)$, and a marginal PDF, $\widetilde{P}(Z)$, as

$$\widetilde{P}(Z, \lambda) = \widetilde{P}(\lambda|Z) \widetilde{P}(Z) \ . \tag{6}$$

It is possible to solve a PDF-transport equation for $\widetilde{P}(Z, \lambda)$ and then integrate Eq. 5 in order to obtain $\widetilde{\boldsymbol{\phi}}$. The FPV model, as proposed by Pierce & Moin,[2,3] is based on a presumed PDF method. It has been

shown by several authors that the PDF of a passive scalar such as the mixture fraction can reasonably be approximated by a beta distribution.[8–10] However, it is well known that PDF's of reacting scalars cannot usually be simply represented by presumed distributions. Pierce & Moin[2,3] have used a beta distribution for the marginal PDF of the mixture fraction. Similar to Janicka & Kollmann,[11] they assumed λ and Z to be independent and chose a delta function for the PDF of λ.

B. Unsteady Flamelet/Progress Variable Model

As described in the previous section, the commonly used steady flamelet model parameterizes the flamelet solutions by the mixture fraction and the stoichiometric scalar dissipation rate, while the parameterization for the flamelet/progress variable model is by mixture fraction and a reactive scalar, characterized by the flamelet parameter λ. Both methods are restricted to the steady flamelet solutions, which is an apparent drawback of these models, since extinction and reignition phenomena in a turbulent flow will lead to transient states away from the steady solutions. It is also clear from Fig. 1 that for these models, the flamelet parameter, which is similar to the stoichiometric temperature, and the stoichiometric scalar dissipation rate have a direct dependence along the S-shaped curve, while in a turbulent flow, a fast change of the scalar dissipation rate might not be followed instantaneously by the corresponding temperature change.

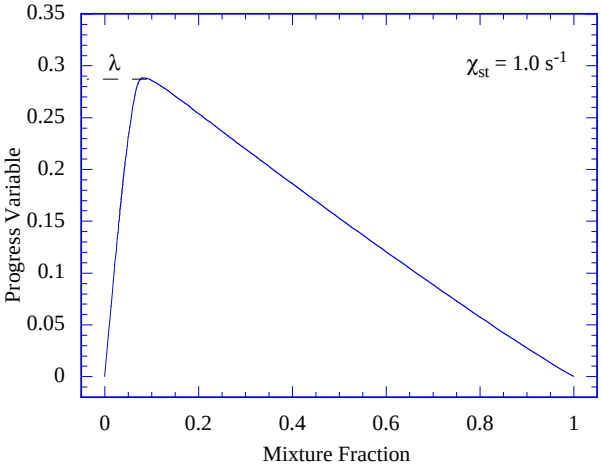

Figure 2. Progress variable as function of mixture fraction for $\chi_{\rm st} = 1.0\,{\rm s}^{-1}$ and definition of the progress variable.

In the unsteady flamelet/progress variable model, both the flamelet parameter and the stoichiometric scalar dissipation rate appear as independent parameters for the flamelet library in addition to the mixture fraction. The unsteady flamelet library is constructed by computing extinguishing and reigniting flamelets. The resulting library is shown in Fig. 1. It has been shown by Pitsch and Fedotov[12] that the rate of change of the temperature is positive on the left side of the S-shaped curve and negative on the right side of the S-shaped curve. This means that an unsteady calculation from the highest to lowest temperature can only be performed at dissipation rates higher than the extinction limit. For lower values, the simulations have been started using the steady state solutions on the unstable branch of the S-shaped curve as initial conditions. The scalar dissipation rate used for the unsteady solution is slightly lower than that of the steady state solution. Since the middle branch is unstable, the temperature will increase and the flamelet solution will approach that of the upper stable branch of the S-shaped curve. Similarly, the part of the flamelet library at lower stoichiometric temperatures is computed starting from a scalar dissipation rate slightly higher than that of the steady flamelet used as initial solution. The part above the upper branch of the S-shaped curve is computed using steady solutions at scalar dissipation rates lower than the considered one as initial conditions. Again, with time, the flamelet temperature will approach the upper stable branch of the S-shaped curve.

After all the required unsteady flamelet solutions are produced, a flamelet library for use in the LES computation is generated. The flamelets are parameterized by mixture fraction Z, flamelet parameter λ, and stoichiometric mixture fraction $\chi_{\rm st}$. Since the flamelet solutions depend only on time, mixture fraction, and stoichiometric scalar dissipation rate, this parameterization eliminates the time as a parameter by introducing the flamelet parameter λ. The flamelet solutions for all scalar quantities $\boldsymbol{\phi}$ can then be given as

$$\boldsymbol{\phi} = \boldsymbol{\phi}(Z, \lambda, \chi_{\rm st})\,. \tag{7}$$

For the further evaluation of the filtered quantities, the joint pdf of the three parameters $\widetilde{P}(Z, \lambda, \chi_{\rm st})$ is required. The filtered scalar values are then given as

$$\widetilde{\phi} = \int_{\lambda^-}^{\lambda^+} \int_0^{\lambda_{\rm max}} \int_0^1 \phi(Z, \lambda, \chi_{\rm st}) \widetilde{P}(Z, \lambda, \chi_{\rm st}) dZ d\lambda d\chi_{\rm st}\,. \tag{8}$$

As described above, the flamelet parameter has been defined in a way that it is independent of the mixture fraction, if the flamelet assumption is valid. The stoichiometric scalar dissipation rate is defined in a similar way by the relation

$$\chi = \chi_{\rm st} f(Z)\,, \tag{9}$$

where $f(Z)$ describes the mixture fraction dependence of the dissipation rate and is taken here from the analytic solution of an unsteady mixing layer.[6] Again, the assumption that Eq. 9 describes the mixture fraction dependence of the dissipation rate implies that $\chi_{\rm st}$ is independent of the mixture fraction. The pdf can then be written as

$$\widetilde{P}(Z,\lambda,\chi_{\rm st}) = \widetilde{P}(Z)\widetilde{P}(\lambda,\chi_{\rm st})\,, \tag{10}$$

As shown by many autors,[8–10] the marginal pdf of the mixture fraction can well be described by a beta-function, which can be determined from the mean and the variance of the mixture fraction. A further assumption here is that λ and $\chi_{\rm st}$ are independent and that the marginal pdfs of both are described by delta-functions. The joint pdf is then modeled as

$$\widetilde{P}(Z,\lambda,\chi_{\rm st}) = \beta(Z;\widetilde{Z},\widetilde{Z''^2})\delta(\lambda-\lambda^*)\delta(\chi_{\rm st}-\chi_{\rm st}^*)\,, \tag{11}$$

The values of λ^* and $\chi_{\rm st}^*$ can be determined from the filtered quantities by the inversion of the integrals

$$\widetilde{C} = \int_0^\infty \int_{\lambda^-}^{\lambda^+} \int_0^1 C(Z,\lambda,\chi_{\rm st})\beta(Z;\widetilde{Z},\widetilde{Z''^2})\delta(\lambda-\lambda^*)\delta(\chi_{\rm st}-\chi_{\rm st}^*)dZ\,d\lambda\,d\chi_{\rm st}\,. \tag{12}$$

and

$$\widetilde{\chi} = \int_0^1 \chi_{\rm st}^* f(Z)\beta(Z;\widetilde{Z},\widetilde{Z''^2})dZ\,. \tag{13}$$

The filtered values $\widetilde{Z}$, $\widetilde{C}$, $\widetilde{Z''^2}$, and $\widetilde{\chi}$ are known from the solution of the filtered transport equations and models for the variance and dissipation rate. In principle, λ^* and $\chi_{\rm st}^*$ could be determined in an iterative procedure by varying their values and evaluating Eqs. 12 and 13 until the integrals yield the mean values. Ultimately, we are interested in the filtered values of the scalars. Here, we first tabulate these values determined from Eq. 8 as function of $\widetilde{Z}$, $\widetilde{Z''^2}$, λ, $\chi_{\rm st}$. These include the filtered values for the reaction progress variable and the scalar dissipation rate $\widetilde{C}$ and $\widetilde{\chi}$. This table could then be used in an LES. For each cell, the values of λ^* and $\chi_{\rm st}^*$ would have to be computed from Eqs. 12 and 13. However, here we take a different approach. For computational efficiency, we re-interpolate the table to a different set of independent parameters. We replace λ by $\widetilde{C}$ and $\chi_{\rm st}$ by $\widetilde{\chi}$. Then, the flamelet library provides the filtered scalars as function of $\widetilde{Z}$, $\widetilde{Z''^2}$, $\widetilde{C}$, and $\widetilde{\chi}$, which are all known as part of the LES solution. Thereby, λ and $\chi_{\rm st}$ are completely eliminated from the computation.

III. Model Validation

A. Experimental Configuration

The experimental study used for the validation of the simulation methodology is the coaxial jet combustor configuration of Spadacchini et al.[13] This experiment was chosen for its relatively simple geometry and boundary conditions, yet complex flow patterns resembling those in a gas turbine combustor, and for the availability of detailed measurements that map the species, temperature, and velocity fields within the combustor. The experimental study consisted of eight test cases conducted under various operating conditions and geometric modifications. The particular case used for the present validation is referred to as "Test 6" in the laboratory report. The geometry is depicted in Fig. 3. The configuration has a relatively large diameter, low velocity central fuel port, with higher velocity, swirling air in a surrounding annulus. The air was preheated to 750 K, the fuel was at 300 K, and the combustor pressure is 1.0 atm. Porous-metal discs were installed in the fuel injector and air entry section to provide uniform inlet flows. The walls of the combustor were water-cooled to maintain a constant wall temperature of roughly 500 K. The dimensions and flow conditions specified in the experiment are summarized in Table 1. The fuel used in the experiment

central pipe radius (R_1):	3.157 cm
annular inner radius (R_2):	3.175 cm
annular wall thickness ($R_2 - R_1$):	0.018 cm
annular outer radius (R_3):	4.685 cm $\equiv R$
combustor radius (R_4):	6.115 cm
combustor length:	100.0 cm
mass flow rate of fuel:	0.00720 kg/s
mass flow rate of air:	0.137 kg/s
bulk velocity of fuel (V_1):	0.9287 m/s
bulk velocity of air (V_2):	20.63 m/s $\equiv U$
swirl number:	0.6
overall equivalence ratio:	0.9
temperature of fuel:	300 K
temperature of air:	750 K
combustor pressure:	1.0 atm

Table 1. Experimental setup and conditions

was natural gas but for the present investigation was assumed to be pure methane. Also, dry air was assumed. The experimental data include radial profiles taken at usually four axial stations, of selected species mass fractions (measured using a traversing gas sampling probe), temperature (measured by a traversing thermocouple), axial and swirl velocities (measured by laser Doppler velocimetry).

Figure 3 also shows a schematic of the flame configuration observed in the experiment. Because of the high air/fuel velocity ratio and the swirl, a strong central recirculation zone is formed directly in front of the fuel port. The recirculating combustion products provide a continuous ignition source for the relatively cold incoming reactants, thereby stabilizing the flame. The flame location, shown as a thick convoluted line in Fig. 3, was observed in the experiment to lift off from the burner and reattach intermittently, in a highly unsteady manner. The length of the flame, as well as the computational domain used for the simulations extends beyond the experimental test section.

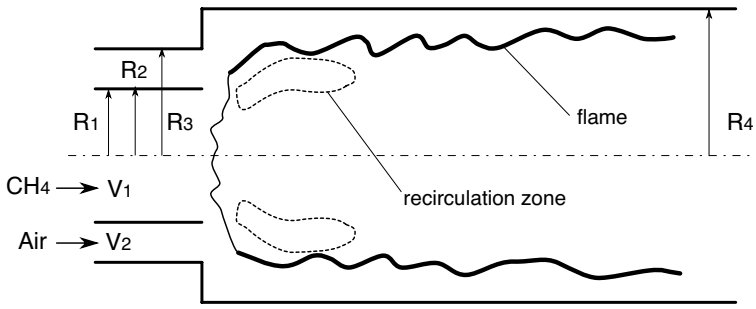

Figure 3. Schematic of the coaxial jet combustor experiment.

B. Numerical Simulation

A large-eddy simulation has been performed for thi test case. The simulation has been performed on a structured cylindrical mesh consisting of 320×150×64 computational cells in axial, radial, and azimuthal direction. The mesh is shown in Fig. 4. The computer code used in this study has been developed at the Center for Turbulence Research by Pierce and Moin.[2,14] The filtered low Mach number approximation of the Navier-Stokes equations is solved in cylindrical coordinates on a structured staggered mesh. The numerical method is a conservative, second-order finite-volume scheme. Second-order semi-implicit time advancement is used, which alleviates the CFL restriction in regions where the grid is refined. Details of the numerical method can be found in Pierce[2,3] and Akselvoll and Moin.[15] All sub-filter quantities have been computed using dynamic models.[16] The flamelet library has been computed using the GRI 2.11 mechanism.[17]

C. Computational Results

The results of the reactive flow simulation using the unsteady flamelet/progress variable model are shown in Figs. 5–11.

To provide a general overview of the reactive flow field, some instantaneous fields from the results of the simulation are shown in Fig. 5. All figures show the upper half of a 2D cut through the combustor. Hence, the lower edge of each figure is the centerline. The flow is going from left to right. The outer inflow is the air stream, the inner inflow is the fuel stream. Note that the fields are not symmetric around the centerline, since all simulations discussed here are time-dependent and 3D. The figures show from top to bottom the axial velocity with the contour of stoichiometric mixture indicated as a black line, the density, the progress variable, and the chemical source term of the progress variable. From the axial velocity it is apparent that there is a recirculation region in the outer part of the flow field, but not at the centerline. This is qualitatively different from the non-swirling case, which shows a recirculation region around the centerline. This is in agreement with the experimental findings, which will be shown below. It can also be observed both from the velocity and from the density field that this recirculation extends into the fuel nozzle, which has also been found in the experiments. The distribution of the progress variable shown in the same figure indicates that the flame is lifted off the nozzle, although stoichiometric conditions exist up to the nozzle rim. The last panel in this figure shows that the chemical source term in the progress variable equation appears in thin layers, even in the downstream regions. Note that the magnitude of the source term depends on the filter size, since a thin flame sheet will lead to a larger filtered source term for a smaller cell than the same flame sheet will for a larger cell.

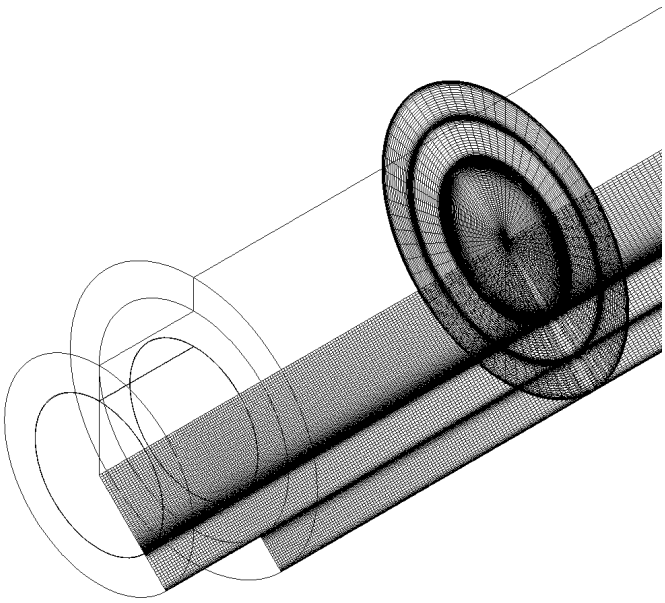

Figure 4. Computational mesh.

The profiles for the axial and swirl velocity are given in Figs. 6 and 7, respectively. The figures show that both the mean and the RMS of the axial velocity are essentially well predicted, especially in the region close to the nozzle. In particular, the location of the recirculation region is well predicted. As mentioned earlier, the recirculation occurs only off-axis and the velocity around the centerline remains positive. However, at the first station, the swirl cone angle seems to be slightly underpredicted. This also seems to be observable from the swirl velocity at this station shown in Fig. 7.a. Further downstream, at $x/R = 1.06$, again, both the mean and the RMS of the velocity components are generally well predicted. Only the computed mean tangential velocity is lower than the experimental data. However, since the overall swirl velocity is well computed upstream and downstream of this location, this error might be attributed to experimental uncertainties. At the even further downstream position at $x/R = 4.05$, the axial velocity at the centerline is overpredicted. However, although slightly weaker, also the experimental data shows an elevated centerline velocity. The same features can be observed in the next downstream position. However, at this position, the overprediction of the centerline axial velocity is even stronger.

The temperature profiles are given in Fig. 8. The experimental data show substantial scatter. In the display of the measured data, for instance in Fig. 8.a, clearly two profiles can be seen. The reason for this is that the data have been measured throughout the entire cross-section of the combustor. Here, we show the data for both halfs of the combustor. The differences between the two profiles are an indication of the repeatability of the experiment. For all four stations, considering these uncertainties, the data are predicted quite accurately. However, at the first station, there is a slight overprediction of the temperature around the centerline of the combustor.

Figure 9 shows the CO_2 mole fraction. The CO_2 mole fraction is underpredicted at the first station. The reason is that the flame stabilization region shows a strongly dynamic behavior. The progress variable

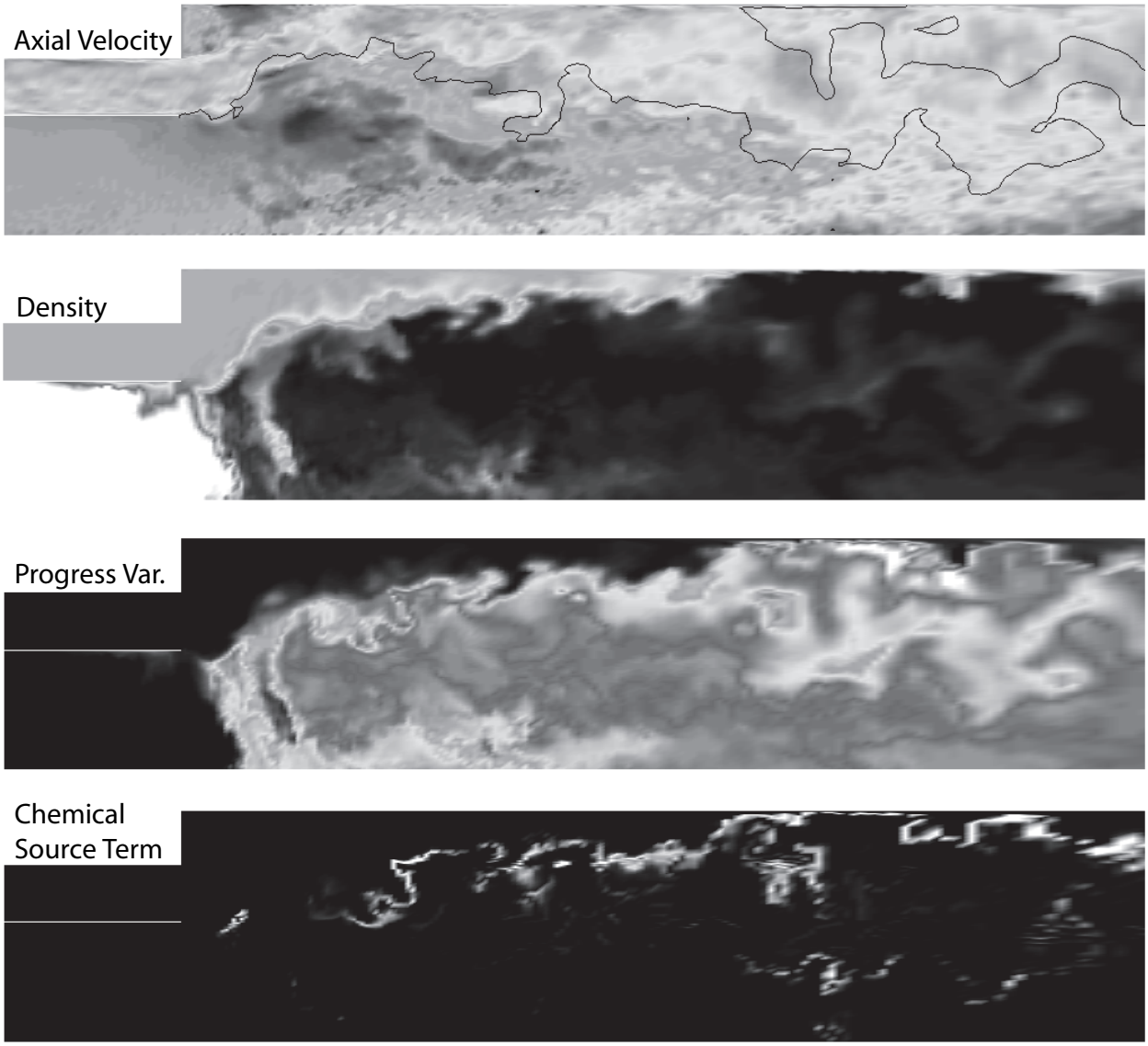

Figure 5. Instantaneous fields of the simulation results. Only one half of the combustor is shown. The lower edge of each figure corresponds to the centerline. Note that this is not a symmetry-line, since the simulations are three-dimensional. From top to bottom: Axial velocity, density, progress variable, chemical source term of the progress variable. The black line in the upper figure denotes stoichiometric mixture.

field shown in Fig. 5 shows a slight lift-off, but burning occurs almost immediately downstream of the nozzle. At different times, however, the flame stabilizes further downstream. The mean values recorded at the first measurement station therefore includes burning and non-burning instances. The underprediction in the CO_2 mole fraction at the first station shows that either the mean flame position is predicted too far downstream or the fluctuations of the flame position too strongly. Further downstream, the CO_2 mole fraction is still underpredicted, but the accuracy is improved in the downstream profiles.

Figure 10 shows the O_2 mole fractions. The profiles agree very well with the experimental data. Only at the first station, the burnout of oxygen is underpredicted, which is in agreement with the underprediction of the carbon dioxide mole fraction.

Finally, CO is shown in Fig. 11. The CO mole fractions are very well predicted considering the fact that in an overall lean environment, this quantity is very sensitive to the flow conditions. The experiments show that the CO mole fraction increases with distance from the nozzle. This trend is captured quite accurately in

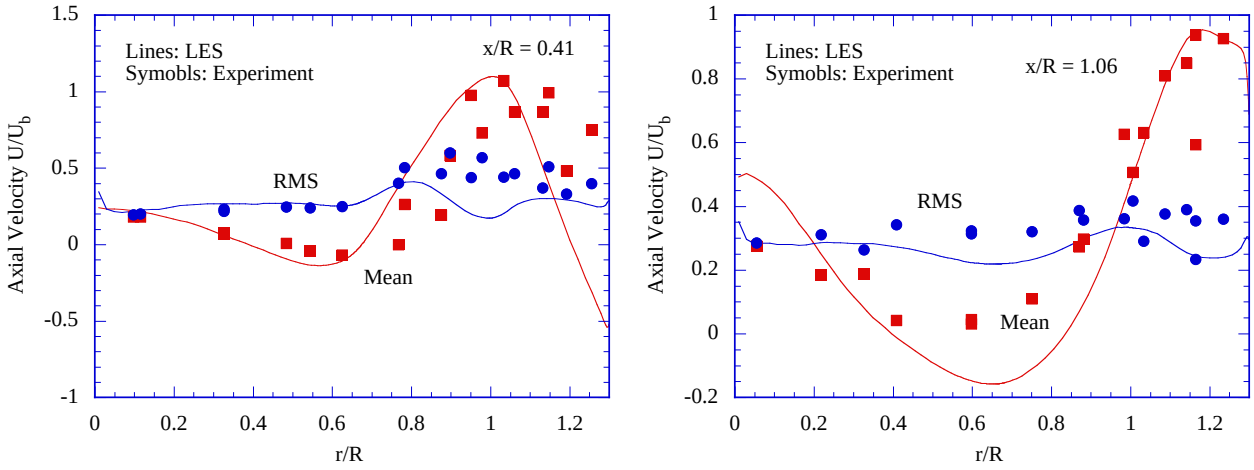

(a) Axial velocity at $x/R = 0.41$

(b) Axial velocity at $x/R = 1.06$

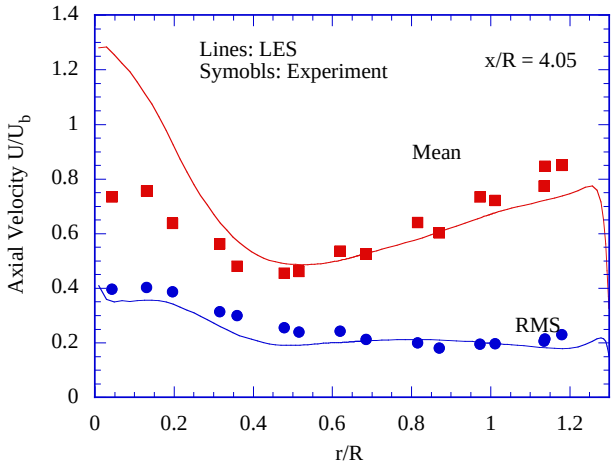

(c) Axial velocity at $x/R = 4.05$

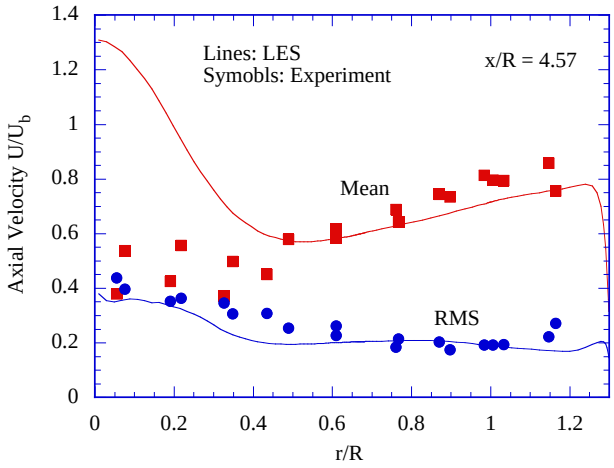

(d) Axial velocity at $x/R = 4.57$

Figure 6. Axial velocity profiles from LES using the extended model compared with experimental data.

the simulations, although the opposite trend could be expected, since in an overall lean environment, mixing should decrease the CO mole fraction. Again, the reason for the lower mean CO mole fraction close to the nozzle is that the Reynolds, or here, the time average includes burning and non-burning regions.

IV. Conclusions

The unsteady flamelet/progress variable model has been developed as a model for aircraft engine combustion and tested with experimental data for the UTRC swirl combustor experiment. The results are in reasonably good agreement with experimental data, even for chemical species, such as CO.

Acknowledgments

Funding from the Department of Energy within the ASC program is gratefully acknowledged.

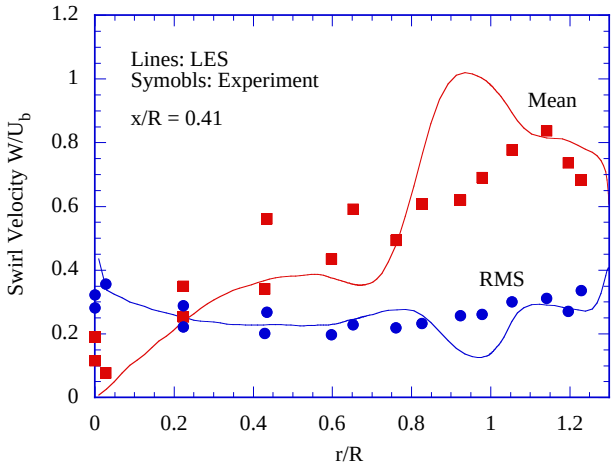

(a) Swirl velocity at $x/R = 0.41$

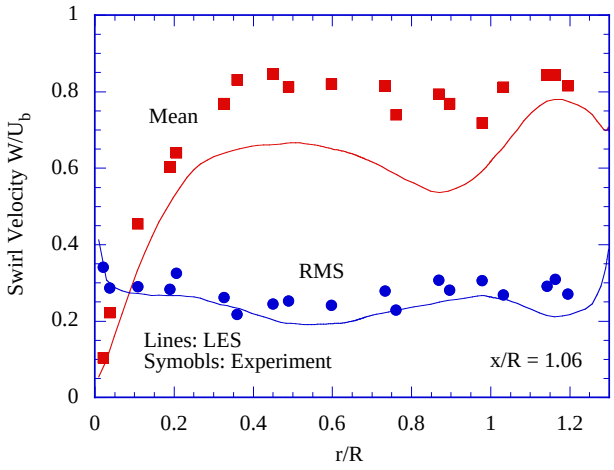

(b) Swirl velocity at $x/R = 1.06$

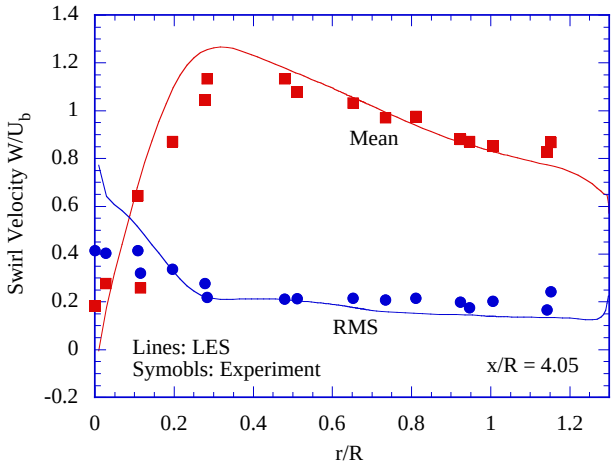

(c) Swirl velocity at $x/R = 4.05$

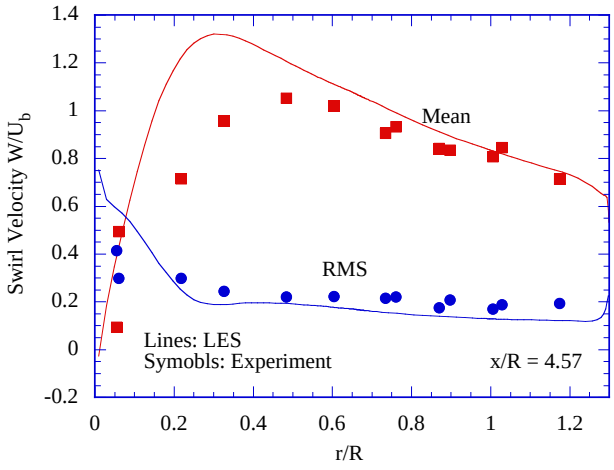

(d) Swirl velocity at $x/R = 4.57$

Figure 7. Swirl velocity profiles from LES using the extended model compared with experimental data.

References

[1]H. Pitsch and H. Steiner. Large-eddy simulation of a turbulent piloted methane/air diffusion flame (Sandia flame D). *Phys. Fluids*, 12(10):2541–2554, 2000.

[2]C. D. Pierce and Moin P. *Progress-Variable Approach for Large Eddy Simulation of Turbulent Combustion*. PhD thesis, Stanford University, 2001.

[3]C. D. Pierce and Moin P. Progress-variable approach for large eddy simulation of non-premixed turbulent combustion. *J. Fluid Mech*, 504:73–97, 2004.

[4]M. Ihme, C. M. Cha, and H Pitsch. Prediction of local extinction and re-ignition effects in non-premixed turbulent combustion by a flamelet/progress variable approach. *Proc. Combust. Inst.*, 30, 2004. to appear.

[5]H. Pitsch. Improved pollutant predictions in large-eddy simulations of turbulent non-premixed combustion by considering scalar dissipation rate fluctuations. *Proc. Combust. Inst.*, 29:1971–1978, 2002.

[6]N. Peters. Laminar diffusion flamelet models in non-premixed turbulent combustion. *Prog. Energy Combust. Sci.*, 10:319–339, 1984.

[7]N. Peters. Local quenching due to flame strech and non-premixed turbulent combustion. *Combust. Sci. Technol.*, 30:1–17, 1983.

[8]A. W. Cook and J. J. Riley. A subgrid model for equilibrium chemistry in turbulent flows. *Phys. Fluids*, 6:2868–2870, 1994.

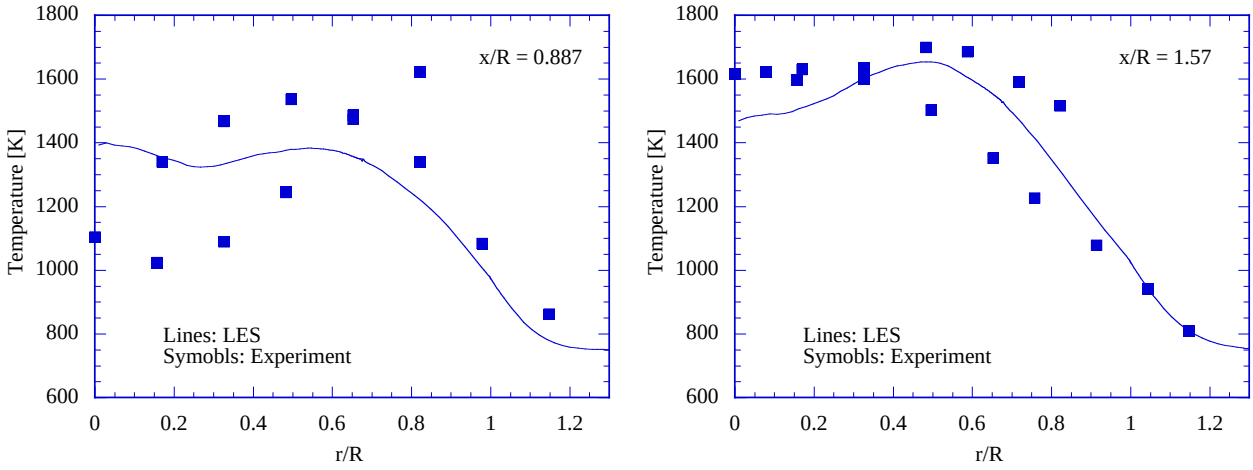

(a) $x/R = 0.887$ (b) $x/R = 1.566$

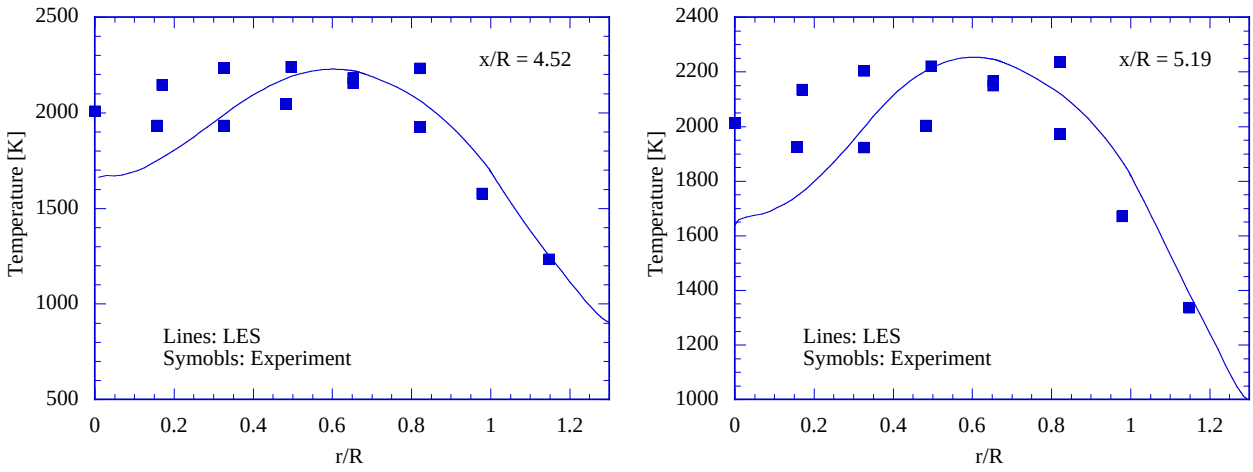

(c) $x/R = 4.515$ (d) $x/R = 5.194$

Figure 8. Temperature profiles from LES using the extended model compared with experimental data.

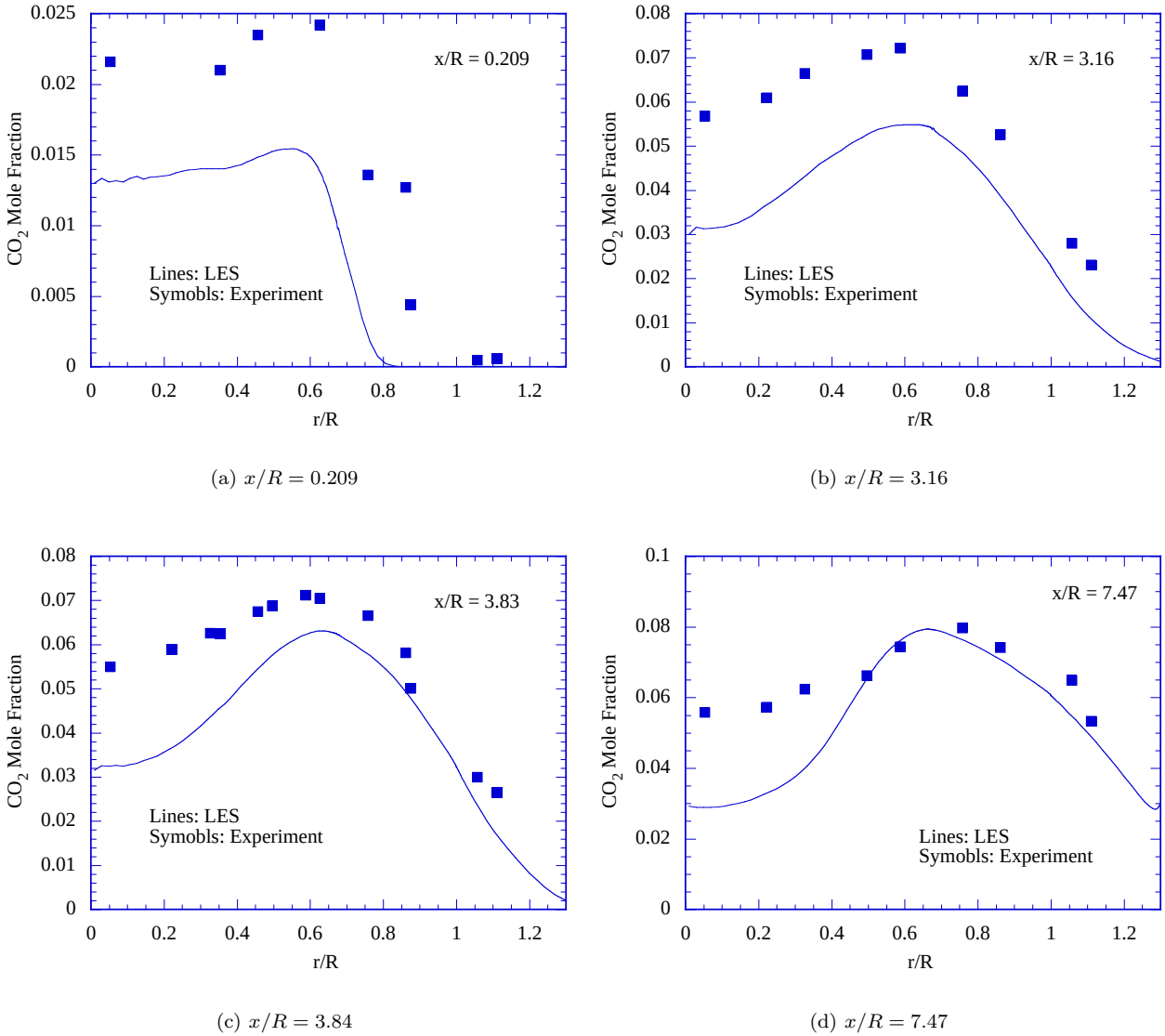

(a) $x/R = 0.209$

(b) $x/R = 3.16$

(c) $x/R = 3.84$

(d) $x/R = 7.47$

Figure 9. CO_2 mole fraction profiles from LES using the extended model compared with experimental data.

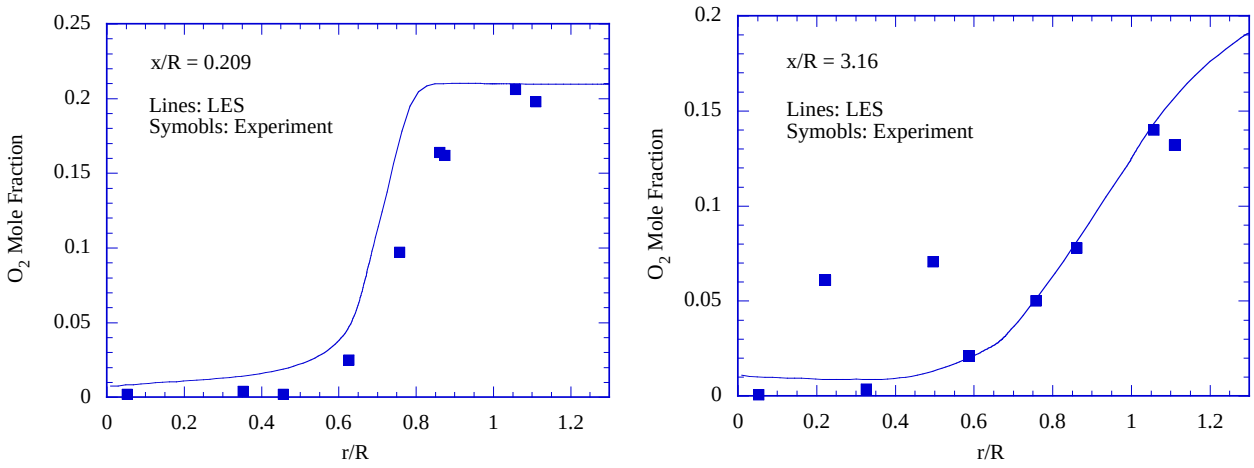

(a) $x/R = 0.209$

(b) $x/R = 3.16$

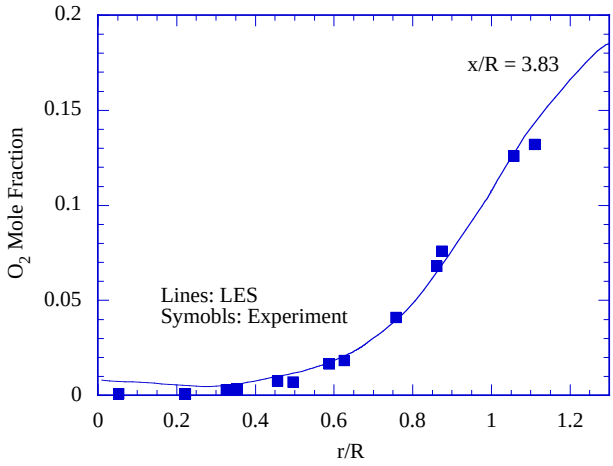

(c) $x/R = 3.84$

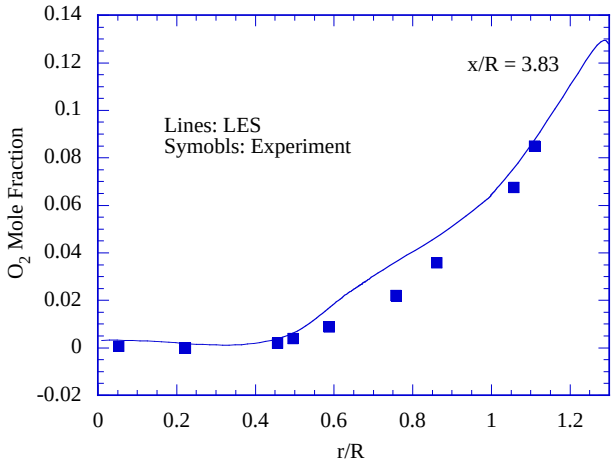

(d) $x/R = 7.47$

Figure 10. O_2 mole fraction profiles from LES using the extended model compared with experimental data.

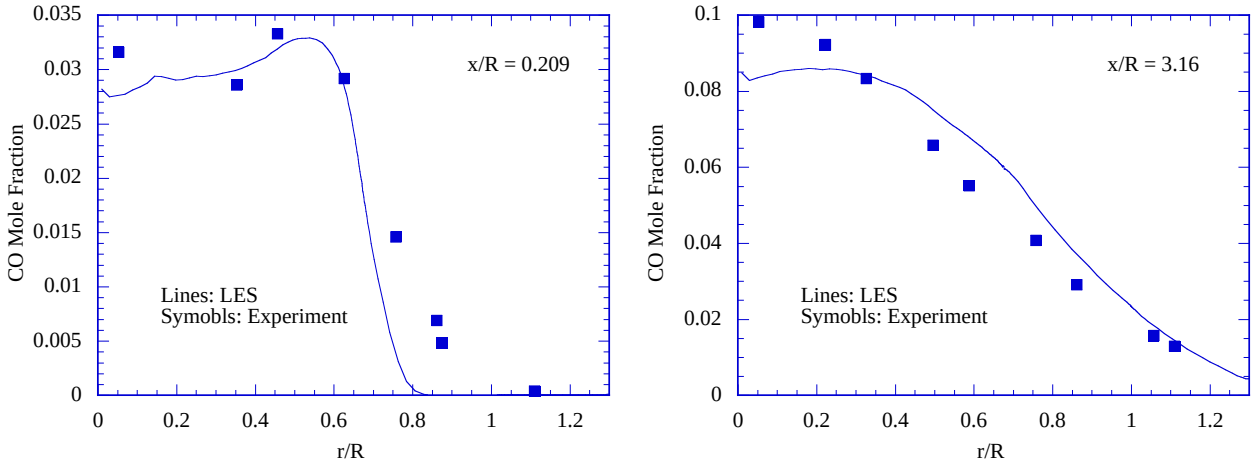

(a) $x/R = 0.209$

(b) $x/R = 3.16$

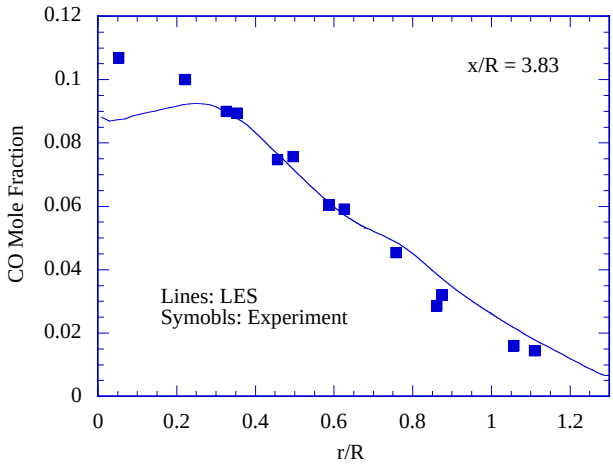

(c) $x/R = 3.84$

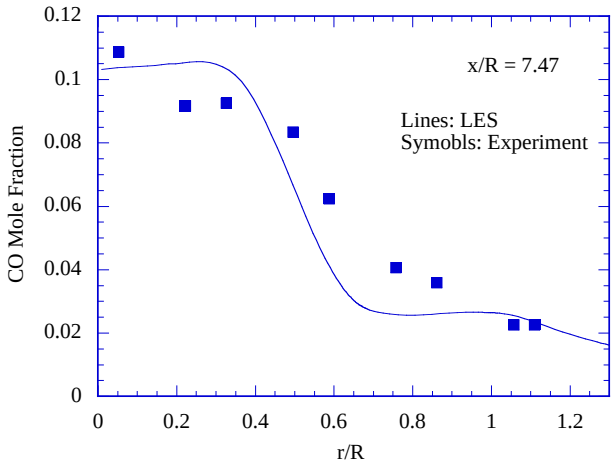

(d) $x/R = 7.47$

Figure 11. CO mole fraction profiles from LES using the extended model compared with experimental data.

[9]J. Jimenez, A. Linan, M. M. Rogers, and F. J. Higuera. A priori testing of subgrid models for chemically reacting non-premixed turbulent shear flows. *J. Fluid Mech.*, 349:149–171, 1997.

[10]C. Wall, B. Boersma, and P. Moin. An evaluation of the assumed beta pdf subgrid-scale model for les of non-premixed,turbulent combustion with heat release. *Phys. Fluids*, 12(10):2522–2529, 2000.

[11]J. Janicka and W. Kollmann. A two-variable formalism for the treatment of chemical reactions in turbulent H_2-air diffusion flames. *Proc. Combust. Inst.*, 17:421–430, 1978.

[12]H. Pitsch and S. Fedotov. Investigation of scalar dissipation rate fluctuations in non-premixed turbulent combustion using a stochastic approach. *Comb. Theory Modelling*, 5:41–57, 2001.

[13]L. J. Spadaccini, F. K. Owen, and C. T. Bowman. Influence of aerodynamic phenomena on pollutant formation in combustion. EPA-600/2-76-247a, 1976.

[14]C. D. Pierce and P. Moin. Large eddy simulation of a confined jet with swirl and heat release. *AIAA Paper*, 98-2892, 1998.

[15]K. Akselvoll and P. Moin. Large-eddy simulation of turbulent confined co-annular jets. *J. Fluid Mech*, 315:387–411, 1996.

[16]P. Moin, K. Squires, W. Cabot, and S. Lee. A dynamic subgrid-scale model for compressible turbulence and scalar transport. *Phys. Fluids A*, 3:2746–2757, 1991.

[17]C. T Bowman, R. K Hanson, D. F Davidson, W. C Gardiner, Jr., V Lissianski, G. P Smith, D. M Golden, M Frenklach, and M. Goldenberg. Gri-mech 2.11. http://www.me.berkeley.edu/gri_mech/, 1995.